

Airframe Design for Silent Fuel-Efficient Aircraft

J. I. Hileman,* Z. S. Spakovszky,† and M. Drela‡

Massachusetts Institute of Technology, Cambridge, Massachusetts 02139
and

M. A. Sargeant§ and A. Jones¶

University of Cambridge, Cambridge, England CB2 1PZ, United Kingdom

DOI: 10.2514/1.46545

The noise goal of the Silent Aircraft Initiative, a collaborative effort between the University of Cambridge and Massachusetts Institute of Technology, demanded an airframe design with noise as a prime design variable and a design philosophy that cut across multiple disciplines. This paper discusses a novel design methodology synthesizing first-principles analysis and high-fidelity simulations, and it presents the conceptual design of an aircraft with a calculated noise level of 62 dBA at the airport perimeter. This is near the background noise in a well-populated area, making the aircraft imperceptible to the human ear on takeoff and landing. The all-lifting airframe of the conceptual aircraft design also has the potential for improved fuel efficiency, as compared with existing commercial aircraft. A key enabling technology in this conceptual design is the aerodynamic shaping of the airframe centerbody. Design requirements and challenges are identified, and the resulting aerodynamic design is discussed in depth. The paper concludes with suggestions for continued research on enabling technologies for quiet commercial aircraft.

Nomenclature

b	= span
C_D	= drag coefficient
C_f	= skin friction coefficient
C_L	= lift coefficient
C_m	= pitching moment coefficient
c	= chord
d	= equivalent diameter for a body of revolution
K	= form factor accounting for pressure drag
L/D	= lift-to-drag ratio
l	= equivalent length for a body of revolution
M	= Mach number
Re	= Reynolds number
S	= planform area
S_{wet}	= wetted area
t	= airfoil thickness
u	= velocity
W	= weight
α	= angle of attack
δ	= wing twist
Λ	= midchord sweep
ρ	= density

I. Introduction

THE heretofore unasked technical question of what an aircraft would look like that had noise as one of the primary design variables calls for a clean-sheet approach and a design philosophy

aimed at a step change in noise reduction. However, with concerns about global climate change growing, fuel efficiency cannot be sacrificed for noise. Although the aircraft noise during takeoff is dominated by the turbulent mixing noise of the high-speed jet, it is the airframe that creates most of the noise during approach and landing. To reduce the aircraft noise below the background noise level of a well-populated area, it is clear that the airframe and the propulsion system must be highly integrated [1] and that the airframe design must consider aircraft operations for slow and steep climbouts and approaches to the airfield [2,3]. Furthermore, the undercarriage must be simple and faired, and high lift and drag must be generated quietly. A candidate configuration with the previously mentioned characteristics is the silent-aircraft experimental design (SAX)-40, as shown in Fig. 1. The conceptual aircraft design uses a blended-wing-body (BWB)-type airframe [4,5] with an embedded boundary-layer-ingesting distributed propulsion system, discussed in depth in a companion paper [6]. The details of the engine design can be found in Hall and Crichton [7,8] and de la Rosa Blanco et al. [9]. The engine inlets are mounted above the airframe to provide shielding of forward-radiating engine noise [10], and the embedding of a distributed propulsion system in the centerbody enables the use of extensive acoustic liners [11].

As depicted in Fig. 1, the airframe design incorporates a number of technologies necessary to achieve the step change in noise reduction. The all-lifting smooth airframe was designed for advanced low-speed capability to reduce noise and efficient cruise performance to improve fuel efficiency. A simple and faired undercarriage, in combination with reduced approach velocities, mitigates the noise generated by unsteady flow structures around the landing gear and struts, as discussed in Quayle et al. [12,13]. To achieve the low approach velocities, deployable drooped leading edges are used in combination with the advanced airframe design. The necessary drag for a quiet approach profile is generated via increased levels of induced drag through an inefficient lift distribution over the all-lifting airframe during approach. This is achieved via a combination of upward-deflected elevons and vectored thrust. Although not used on the conceptual aircraft design presented here, other quiet drag concepts were investigated, which are potentially applicable for conventional aircraft configurations. For example, the acoustic signature of perforated drag plates is reported in Sakaliyski et al. [14], and a novel, quiet engine air-brake concept, based on steady swirling flow to generate pressure drag, is discussed in Shah et al. [15]. The airframe trailing edges are acoustically treated by deploying brushes to reduce the airfoil self-noise. This concept is similar to the quiet flight of the owl, for which the feathers are used to reduce the flow

Presented as Paper 453 at the 45th AIAA Aerospace Sciences Meeting and Exhibit, Reno, NV, 8–11 January 2007; received 29 July 2009; revision received 4 December 2009; accepted for publication 17 February 2010. Copyright © 2010 by the authors. Published by the American Institute of Aeronautics and Astronautics, Inc., with permission. Copies of this paper may be made for personal or internal use, on condition that the copier pay the \$10.00 per-copy fee to the Copyright Clearance Center, Inc., 222 Rosewood Drive, Danvers, MA 01923; include the code 0021-8669/10 and \$10.00 in correspondence with the CCC.

*Principal Research Engineer, Department of Aeronautics and Astronautics, Gas Turbine Laboratory, 77 Massachusetts Avenue. Member AIAA.

†Associate Professor, Department of Aeronautics and Astronautics, Gas Turbine Laboratory, 77 Massachusetts Avenue. Member AIAA.

‡Professor, Department of Aeronautics and Astronautics, Gas Turbine Laboratory, 77 Massachusetts Avenue. Fellow AIAA.

§Ph.D. Student, Engineering Department, Trumpington Street.

¶Ph.D. Student, Engineering Department, Trumpington Street. Member AIAA.

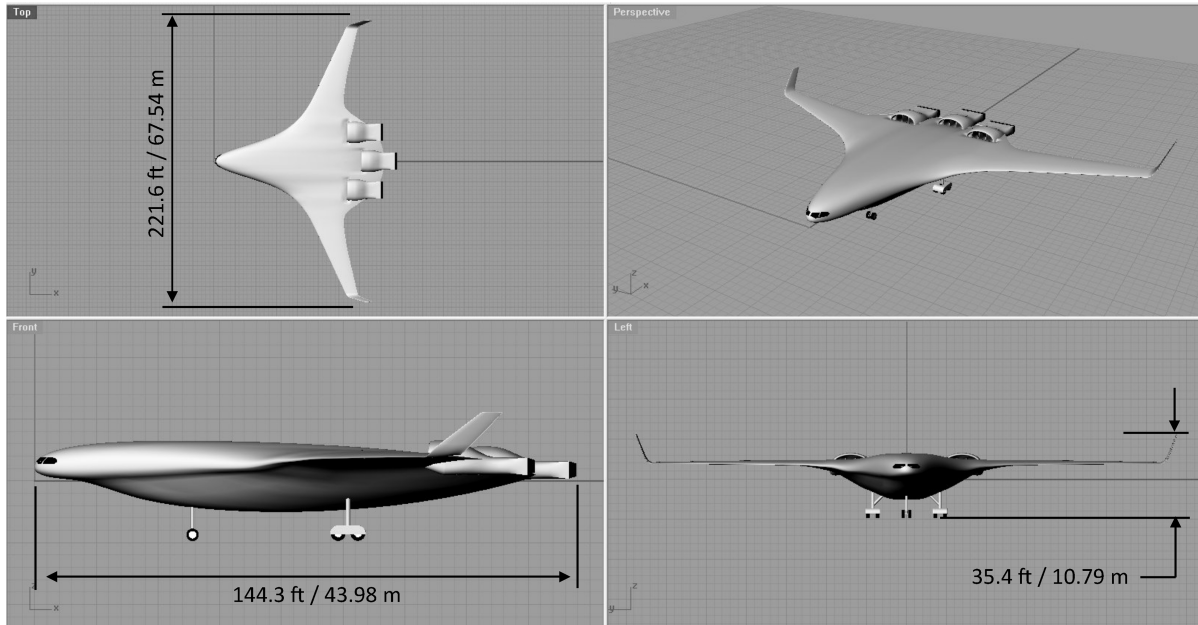


Fig. 1 SAX-40.

noise of the wings, as reported by Lilley [16]. A noise reduction of about 4 dB was experimentally demonstrated by Herr and Dobrzynski [17], using trailing-edge brushes on a scale-model aircraft wing.

The present paper focuses on the detailed airframe design for a step change in noise reduction and improved fuel efficiency. More specifically, the objectives are:

- 1) Establish a newly developed quasi-three-dimensional (3-D) aerodynamic airframe design methodology based on the previously mentioned concepts.
- 2) Validate the methodology using 3-D Navier–Stokes simulations of a candidate airframe design.
- 3) Define and optimize a conceptual aircraft design for low noise and improved fuel efficiency by combining the methodology with noise assessment tools.

The resulting conceptual aircraft design (SAX-40) yields a calculated noise level at the airport perimeter of 62 dBA and has the potential for a fuel efficiency of 124 passenger (pax) miles per gallon, a 28% improvement when compared with existing commercial aircraft. SAX-40 meets the objectives of a silent and fuel-efficient conceptual aircraft design; however, some of the technologies are high risk. In the future, the design methodology that resulted from the SAX design process could be used to further probe the aircraft design space to achieve further reductions in fuel use and emissions while maintaining ultralow noise levels. This methodology thus represents a step toward aircraft design for reduced environmental impact.

The paper is organized as follows. The design requirements and challenges for a silent and fuel-efficient aircraft are discussed first. Next, the key features of the aerodynamic airframe design are outlined, elucidating how a step change in noise reduction and enhanced aerodynamic performance are achieved. The evolution of the airframe design, along with the characteristics of three generations of designs, is briefly summarized. The airframe design methodology and framework used in the last generation of designs is then described in detail. Next, the established aerodynamic design framework is validated using a 3-D Navier–Stokes calculation of a candidate airframe design. The framework is then used to optimize for low noise and improved fuel efficiency, and the resulting design (SAX-40) is discussed in detail. Last, the findings and conclusions are summarized, and an outlook on future work is given.

II. Key Challenges and Enabling Concepts

A key airframe design requirement necessary to achieve the approach-noise goal is the capability of the aircraft to fly a slow

approach profile. The sound pressure levels of the airframe noise sources scale with $1/r^2$ and u^n , where r is the distance between source and observer and u is the approach velocity. The exponent n is five or six, depending on whether the noise stems from scattering of turbulent structures near edges or acoustic dipoles. The scaling law thus suggests that the noise at the observer location can be reduced by using a slow approach profile and by landing further into the runway [3,18] to keep the aircraft at a higher altitude when crossing the airport perimeter. This requires a low stall speed for the airframe and correspondingly increased amounts of drag. The low approach speed determines the landing field length, which combined with the runway length, sets the threshold displacement. Although the conceptual design is strongly governed by noise considerations, fuel economy and emission levels must be competitive with next-generation aircraft. This requirement raises the question of whether tradeoffs between noise and fuel efficiency need to be made and, if so, what the potential penalty for noise reduction is. This paper demonstrates that, by taking advantage of the all-lifting configuration and by aerodynamically shaping the airframe centerbody, both a reduction in noise and an improvement in fuel efficiency can be achieved.

A. Major Challenges

The previously mentioned requirements introduced major design challenges. The first challenge is to achieve competitive cruise performance while maintaining effective low-speed aerodynamic characteristics. For a given aircraft weight, either the area or the lift coefficient need to be increased during landing to reduce the approach velocity. This demands either variable wing geometry, such as achieved with conventional flaps and slats, or circulation control. Conventional flaps and slats are inherently noisy and thus must be avoided. Circulation control [18,16] is a possible option, but the impacts of weight and complexity of the flow control system on overall performance and cruise efficiency would need to be assessed in detail. The idea adopted here is to avoid this complexity and to incorporate passive circulation control in the aerodynamic design of the all-lifting airframe by optimally shaping its centerbody.

To achieve the noise goal, the lifting surfaces must be smooth, and the undercarriage needs to be simple and faired. This inherently reduces the drag on approach, which poses another challenge in the design of a low-noise aircraft. The drag required for a slow approach profile must be generated in quiet ways. The concept used here is to increase the induced drag by setting up an inefficient but relatively quiet lift distribution over the airframe during approach.

Another major challenge lies in trimming and rotating a tailless airframe, such as the all-lifting configuration considered here. Pitch trim and static stability can be achieved without a tail, but they require reflexed airfoils on the centerbody [4]. The major drawbacks thereof are a penalty in cruise performance and relatively large control surfaces and actuation power to facilitate rotation. As discussed next, aerodynamically shaping the leading-edge region of the centerbody enables pitch trim and static stability without the use of reflexed airfoils or canards.

B. Key Airframe Design Feature

It is important to note that the holistic approach and the integrated system design of the SAX-40 are crucial to achieve the noise goal and to improve fuel efficiency. In this, the all-lifting airframe incorporates a key design feature that distinguishes the conceptual aircraft design presented here from other BWB-type concepts. As depicted in Fig. 1, the leading-edge region of the centerbody is aerodynamically shaped, and the all-lifting airframe is optimized to generate a lift distribution that can do the following:

- 1) The airframe can balance aerodynamic moments for pitch trim and provide a 5 to 10% static stability margin while avoiding a horizontal-tail lifting surface and reflexed airfoils.
- 2) The airframe can achieve an elliptical span load on cruise, yielding a 15% improvement in ML/D when compared with current BWB aircraft designs.
- 3) The airframe can increase the induced drag on approach via elevon deflection and vectored thrust, reducing the stall speed by 28% when compared with currently operating airframes.

A companion paper by Sargeant et al. [19] presents a detailed aerodynamic analysis of the SAX-29 design with an explanation of how leading-edge aerodynamic shaping improves the aerodynamic performance of BWB-type aircraft.

III. Airframe Design Evolution

The SAX-40 aircraft design is the culmination of an iterative design process that, in retrospect, evolved from three major aircraft-design generations. In each generation, the assessment tools were further developed to improve fidelity, and the redesigns were aimed at closing the gap between the estimated aircraft performance and the design goals. In conclusion of each of these major design steps, technical reviews were held with The Boeing Company and Rolls-Royce. This section highlights the major characteristics and outcomes of the design evolution.

A. First-Generation Silent-Aircraft Experimental Design

The first generation of SAX designs used a modified version of Boeing's multidisciplinary design optimization code (WingMOD) [4,20], for which the objective function for the optimizer was focused on minimizing takeoff weight. This design process culminated in the SAX-12 planform [5]. As shown in Fig. 2, the configuration incorporates four boundary-layer diverting Granta-252 engines [7,8]. The cruise altitude, Mach number, range, and passenger capacity were held constant for the SAX-12 and subsequent designs. The aircraft design was calculated to have a maximum takeoff weight (MTOW) of 340,150 lb, a fuel efficiency of 88 pax miles per gallon (with 220 lb of payload being allocated to each passenger), and maximum noise levels at the airport perimeter of 80 and 83 dBA during takeoff and approach, respectively [5]. Considerable challenges remained before the noise goal could be achieved; chief among them was the lack of a methodology to optimize the aerodynamic shape for low noise. Thus, a clear need was the

capability to define the 3-D geometry of the airframe and a novel airfoil stack. The SAX-12 planform shape, airfoil thickness distribution, minimum cabin size, rear spar location, and mission were carried over as starting points in the next generation of aircraft design. In addition, WingMOD was used to create the structure-weight response-surface model (RWM) that was used throughout the design process.

B. Second-Generation Silent-Aircraft Experimental Design

The focus of the second generation of SAX designs was the development and validation of a quasi-3-D airframe design methodology with inverse design capabilities. This methodology will be discussed in Sec. IV. For the second generation of designs, this methodology was used to achieve a significant reduction in noise by reducing the stall speed. This resulted in aerodynamic shaping of the centerbody leading edge, with supercritical profiles designed for the outer-wing sections. The design process started with the SAX-15 and culminated in the SAX-29 planform, shown in Fig. 2 in the center. This design incorporated a boundary-layer-ingesting distributed-propulsion system based on three engine clusters. Each engine cluster consisted of a single gas generator driving three fans. To assess the methodology and the effectiveness of the centerbody aerodynamics, a 3-D Navier-Stokes calculation was carried out for the SAX-29 airframe at the Boeing Phantom Works. The details of the analysis are presented in Sec. V. The quasi-3-D design methodology was successfully validated, such that the airfoil profiles and detailed centerbody shape of the SAX-29 design were used in subsequent airframe designs.

C. Third-Generation Silent-Aircraft Experimental Design

The third and last generation of designs focused on further refinement of the aerodynamics and the weight models by taking advantage of the optimization capability of the design methodology. A gradient-based optimization of the outer-wing shape was used to minimize a cost function combining approach noise and fuel efficiency. The outcome of the optimization culminated in the SAX-40 planform, shown in Fig. 2 and discussed at length in Sec. VI. Similar to the second-generation SAX-29 design, the SAX-40 incorporates three Granta-3401 boundary-layer-ingesting engine clusters. The distributed propulsion system consists of three gas generators and nine fans. Engine and transmission-system design details can be found in de la Rosa Blanco et al. [9], and the integration of the propulsion system into the airframe is discussed in Plas et al. [6]. The SAX-40 aircraft design was calculated to have an MTOW of 332,560 lb, a fuel efficiency of 124 pax miles per gallon (with 240 lb of payload being allocated to each passenger), and maximum noise at the airport perimeter of 62 dBA [2,3].

D. Design Comparison

As the SAX design evolved, significant gains in ML/D were achieved, and the approach velocity was reduced while increasing the planform area, as tabulated in Fig. 3. Most of the improvement in ML/D can be attributed to the aerodynamic shaping and cambering of the centerbody leading edge, which enabled a nearly elliptical lift distribution. In addition (as shown in Fig. 3), the optimization process increased the planform area, slightly unswept the wings, and grew the span, yielding a reduction in stall speed. The optimization of the 3-D airframe geometry demonstrates that a configuration with both lowered noise emission and improved fuel efficiency can be achieved. This was not clear before the optimization, as it was



Fig. 2 Three major generations of conceptual aircraft designs: SAX-12, SAX-20, and SAX-40.

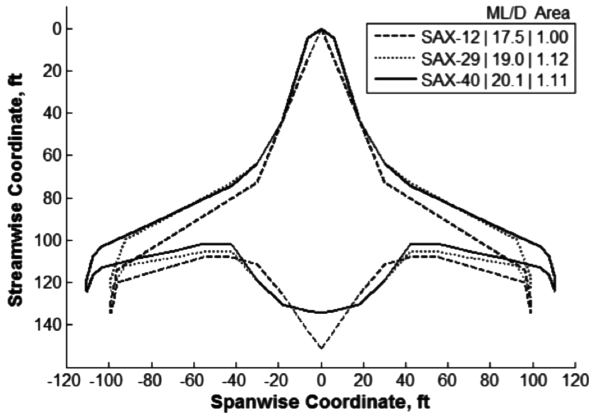


Fig. 3 Evolution of SAX planform and aircraft performance.

hypothesized that cruise performance penalties would have to be incurred for reduced noise [21].

IV. Technical Approach: Quasi-Three-Dimensional Design Methodology

The unconventional airframe configuration yields a highly 3-D aerodynamic design problem that requires a 3-D analysis to capture the centerbody aerodynamics. Viscous 3-D calculations are too costly to fully explore the design space, so a framework with a faster turnaround time but adequate fidelity was developed. A quasi-3-D design methodology was created by combining a two-dimensional (2-D) vortex lattice method with sectional viscous airfoil analyses and empirical drag estimates of the 3-D centerbody, thus enabling rapid design iterations and optimization. At every major design change during this iterative process, a fully 3-D flow assessment was conducted. A 3-D full-panel method (Newpan [22]) and Euler calculation (Fluent) of the entire airframe were carried out to assess

the loading of the airfoils and shock strength. To validate the overall framework and procedures, a 3-D Navier–Stokes calculation was conducted, and the results demonstrated good agreement with the established quasi-3-D design methodology. An outline of the design methodology is given in this section, and the details of the validation are discussed in Sec. V.

The quasi-3-D design methodology, schematically shown in Fig. 4, can be broken into four main parts: 1) 3-D airframe generation, 2) cruise performance analysis, 3) low-speed performance analysis, and 4) nonlinear optimization of the outer-wing shape. The methodology assesses the aircraft design over five mission points: takeoff rotation, takeoff climbout, begin cruise, end cruise, and approach. Each of the four parts of the methodology and their use during the missions is described next.

A. Three-Dimensional Airframe Generation

The 3-D airframe shape is created from the lofting of an airfoil profile stack to conform to a prescribed planform shape. As presented in Fig. 5, four airfoil cross sections and the linear interpolation of adjacent airfoil sections are used to define airfoil profiles at each spanwise location. Unshaded areas within the top-down view of the planform have airfoil profiles created from adjacent regions. Twist and thickness distributions, also shown in Fig. 5, are used to complete the 3-D geometry creation. Bezier splining was used to create the airfoil profiles [23,24]. As shown in Fig. 6, which presents the centerbody and outer-wing airfoil profiles, respectively, the airfoil suction and pressure surfaces of the profile are defined by two and three Bezier splines, respectively. The third Bezier spline shapes the profile and camber near the leading edge. Continuity of the profile slope is ensured at spline intersections. Each airfoil is twisted and scaled to yield the prescribed twist and thickness-to-chord distributions. The lofted airfoil sections are required to enclose the rear spar, the front outer-wing spar, and the passenger cabin.

As shown in Fig. 5, the wing twist was defined over three linear segments with nonzero twist at the aircraft centerline. The shape of the twist distribution was manually refined throughout the design

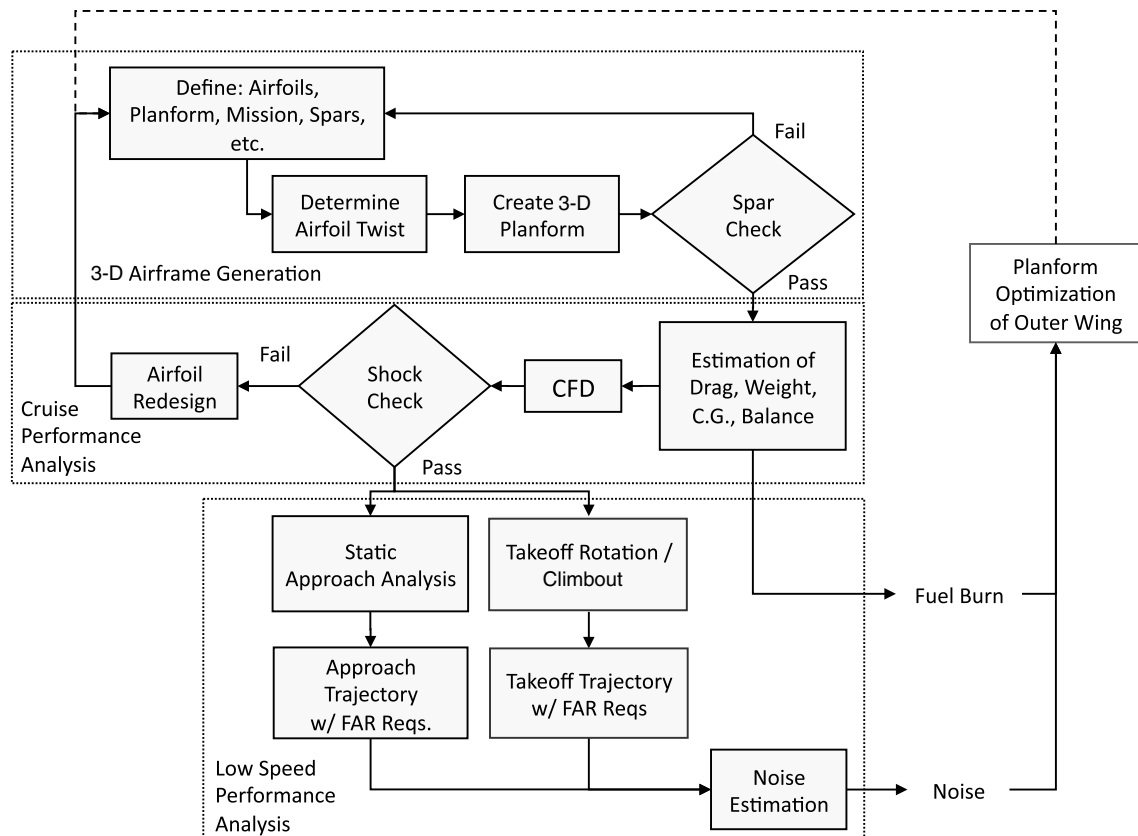


Fig. 4 Quasi-3-D design methodology used in the creation of the SAX-40 planform (FAR denotes Federal Aviation Regulation).

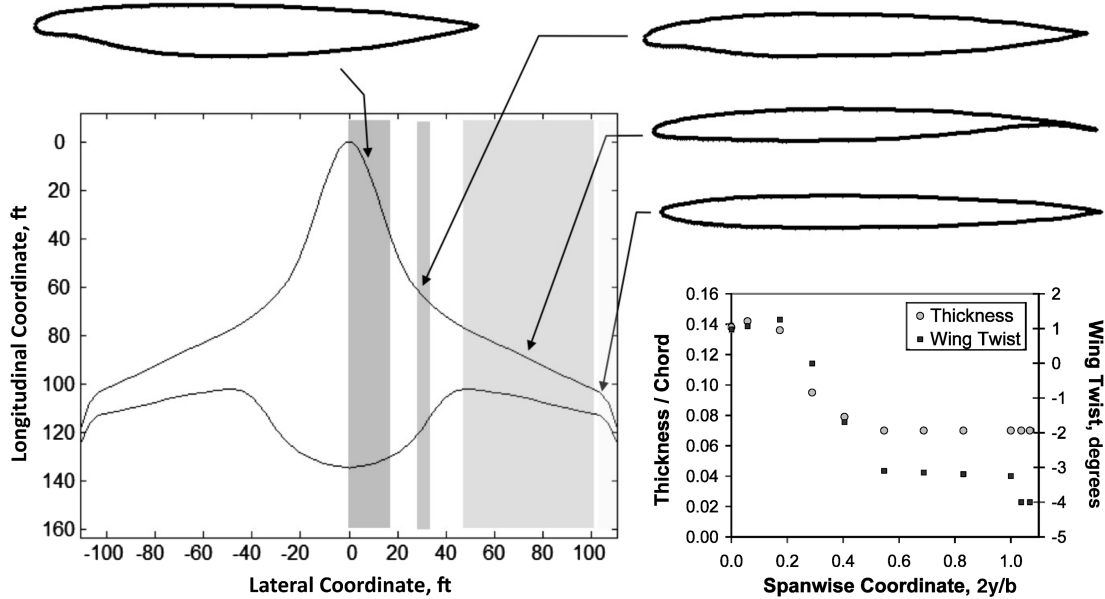


Fig. 5 SAX-40 airfoil sections, planform shape, and distributions of twist and airfoil thickness.

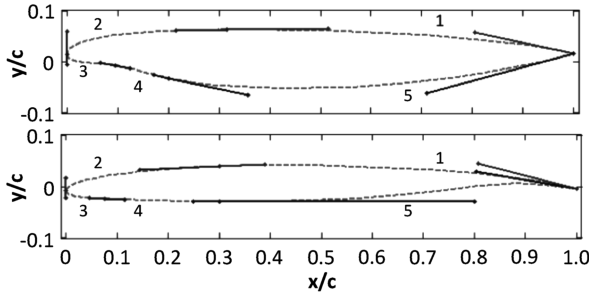


Fig. 6 Centerbody and outer-wing airfoils for the SAX-40 design and the five Bezier splines used in their creation. The vectors that define the five Bezier splines are also shown.

process. The magnitude of the twist distribution was scaled to yield a zero-net pitching moment at the beginning of cruise. A vortex lattice code with aerodynamic, trim, and stability analyses (AVL) was used for this purpose [25]. Two geometries with different maximum wing twists were analyzed with AVL. The linear variation of C_L and C_m , with angle of attack and outer-wing twist, form two equations that can be solved for the angle of attack and outer-wing twist required for $C_m = 0$ and $C_L = W/(\frac{1}{2}\rho u^2 S)$, where W is the MTOW. This can be mathematically expressed as

$$\begin{bmatrix} \frac{\partial C_L}{\partial \alpha} & \frac{\partial C_L}{\partial \delta_t} \\ \frac{\partial C_m}{\partial \alpha} & \frac{\partial C_m}{\partial \delta_t} \end{bmatrix} \begin{bmatrix} \Delta \alpha \\ \Delta \delta_t \end{bmatrix} = \begin{bmatrix} C_L - C_{L,\alpha_0} \\ C_m - C_{m,\delta_{t,0}} \end{bmatrix} \quad (1)$$

where the actual angle of attack and outer-wing twist are:

$$\alpha = \alpha_0 + \Delta \alpha; \quad \delta_t = \delta_{t,0} + \Delta \delta_t \quad (2)$$

This twist distribution is used to define the aircraft.

B. Cruise Performance Analysis

The methodology iteratively estimates the aerodynamic performance using the procedure outlined next.

1. Cruise Drag

The airframe drag was estimated from the output from AVL and MSES v3.02 (a 2-D compressible, viscous airfoil design and analysis tool [26–28]), combined with empirical relations. The total drag on the aircraft is computed from the summation of the lift-induced drag,

the pressure drag, the skin-friction drag, and the wave (compressibility) drag from the centerbody, the midwing, the outer wings, the winglet, and the engine nacelles. The induced drag for the airframe is estimated using AVL. The drag reduction from boundary-layer ingestion [6,24] that results from embedding the propulsion system is book-kept within the thrust-specific fuel consumption (SFC).

The pressure and friction drag from the centerbody are estimated using compressibility corrected, empirical relationships by Hoerner [29] for bodies of revolution measured at a high Reynolds number Re approaching 10^{10} . The centerbody region is converted to a body of revolution with equivalent surface area. The combined pressure and friction drag coefficients from such a body of revolution can be approximated by

$$C_{D,wet} = \left[\frac{0.03}{Re^{1/7}} + \frac{0.0016}{Re^{0.4}(d/l)} \right] \times [1 - 0.09M^2][1 + 1.15(d/l)^{1.5} + 6(1 - M^2)^{-0.6}(d/l)^3] \quad (3)$$

where the diameter-to-length ratio d/l for the airframe is computed by dividing the equivalent diameter by the centerbody chord. The equivalent diameter is that required to have an area equivalent to the centerbody cross section at its maximum thickness,

$$d/l = \frac{1}{c_1} \sqrt{\frac{8b(c)\langle t/c \rangle}{\pi}} \quad (4)$$

where b and c_1 denote the centerbody span and chord, respectively. The expressions within the first bracketed term of Eq. (3) are the skin friction coefficient for a 3-D body of revolution with a Reynolds number between 10^7 and 10^9 . The second bracketed term corrects the skin-friction coefficient for compressibility, assuming a smooth surface. The third bracketed term, when multiplied by the skin-friction coefficient, approximates the friction plus pressure drag coefficients of a conventional body of revolution, which is defined by a maximum diameter of 30 to 40% of the body length. The drag coefficient of Eq. (3) is based on a wetted surface area of a streamlined body and is approximated by

$$S_{wet} = 3S_0(d/l)^{-1} \quad (5)$$

where S_0 is the surface area of the centerbody region.

The pressure, friction, and wave drag for the outer wings and winglets are estimated using MSES on swept airfoil sections that have an angle of attack adjusted to yield the sectional C_L for that airframe section. The pressure drag from the MSES analysis of the

swept airfoil is converted to that of an unswept airfoil by $C_{Dp} = C_{Dp,swept} \cos^3 \Lambda$ [29].

The drag from the engine nacelles is computed using

$$C_{D,nacelle} = K C_f \frac{S_{wet}}{S} \quad (6)$$

where K is a form factor that accounts for pressure drag. It is estimated according to [30]

$$K = 1 + 0.35/(L/D) \quad (7)$$

where L is the nacelle length, D is the nacelle diameter, and C_f is the skin-friction coefficient estimated from relations given by [29]

$$C_f = 0.455/[\log_{10}(Re)]^{2.58} \quad (8)$$

where the Reynolds number is based on nacelle length. The wetted nacelle area S_{wet} is estimated from the inlet and nacelle geometry.

2. Weight

The MTOW for the aircraft was estimated as the summation of the design payload, the operating empty weight (OEW), and the fuel weight. The design payload was defined as 215 pax with a total weight allotment of 240 lb/pax (passenger weight of 195 lb plus 45 lb of luggage). The aircraft OEW was created from estimates of structures, propulsion system, landing gear, and fixed equipment. The structural weight was estimated using a least-squares quadratic RSM that was created from several WingMOD [31] designs. The RSM is defined by the functional relationship,

$$W_s = \phi_1 W_f + \phi_2 W_p + \phi_3 S \quad (9)$$

where W_s , W_f , W_p , and S are the structural weight, fuel weight, propulsion system weight, and wing area, respectively. The coefficients ϕ_i were determined using a least-squares fit, as described in Diedrich [32]. The structure weight for the SAX-40 was updated from that given previously, and it assumed a 10% improvement in composite material weight by 2025. The propulsion-system weight was quantified using the model described in de la Rosa Blanco et al. [9], for which the weights were estimated for all of the engine subcomponents, the transmission system, the cooling system, the engine support, and the thrust vectoring nozzle. The landing-gear weight was estimated as 4% of the MTOW plus 660 lb for fairings, as estimated by Jones [23]. The fixed-equipment weight was estimated using a semiempirical statistical scaling model, modified from Roskam [33], with details provided in Jones [23]. The final weights the model deviated from that described in Jones [23], in that the auxiliary power unit was set as 1,500 lb, and a half gallon of water was allocated per passenger.

The fuel weight was composed of climb fuel, mission fuel, reserve fuel, and unusable fuel. The climb fuel was assumed to be 2% of MTOW. The mission fuel was estimated from the cruise velocity, the average cruise thrust (determined from the aircraft weight and ML/D for both beginning and end cruise), and average cruise SFC, which incorporated the engine performance and the influence of boundary-layer ingestion [6,9]. The reserve fuel was estimated from flying 200 n mile and 0.75 h at the end-cruise fuel-burn rate. The unusable fuel was set as 1% of the summation of the climb, mission, and reserve fuel weights.

3. Aircraft Balance

The center of gravity of the aircraft was estimated for each of the five mission points, using the center of gravity and weights of the systems, the payload, the fuel, the propulsion system, and the structure. The center of gravity of the structure was estimated as the airframe center of volume, assuming a uniform density of the airframe materials. The payload was placed with the centers of volume of the cabin and cargo bay. The engines were placed, such that the Mach number at the inlet would be below 0.85. The fixed-equipment weight was placed in the cabin, cargo bay, structure, and nose of the aircraft, as appropriate. The landing gear was placed on

the airframe, such that rotation was assured and tail strike avoided. Detailed information on the undercarriage can be found in Quayle et al. [12,13].

4. Validation of Aerodynamic Design Using Computational Fluid Dynamics

Throughout the design process, intermediate aircraft designs were examined with higher-fidelity computational-fluid-dynamics (CFD) tools to better understand the aircraft performance and to improve the design process. Three computational models were employed for this purpose: a 3-D Euler solution, an inviscid full panel solution, and a viscous 3-D solution to the full Navier–Stokes equations. The validation step is discussed at length in Sec. V.

5. Airfoil Design

If the CFD validation revealed the presence of strong shocks or Mach numbers in excess of 1.15, the 2-D airfoil profiles were manually altered to improve the aircraft performance. To accurately capture the flow over the aircraft, the outer-wing profiles were modified by the midchord sweep angle Λ , because the flow in this region is largely 2-D, with fluid motion normal to the midchord line. The lift coefficient, Mach number, and local airfoil thickness are affected by the sweep angle according to $C_{L,swept} = C_L/\cos^2 \Lambda$, $M_{swept} = M \cos \Lambda$, and $y_{swept} = y/\cos \Lambda$ [29]. The flow over the centerbody is highly 3-D with considerable pressure relief, so there is no obvious choice for a sweep angle. The centerbody airfoil design thus used an unswept profile through the center of the aircraft.

The airfoil design process resulted in two distinctly different profiles for the outer wings and the centerbody. The outer-wing profile achieves low-cruise drag (see Fig. 7) with high lift at approach speeds (Fig. 8). This combination allows for efficiency at cruise (which results in reduced fuel use) and for reduced speeds during takeoff and approach (which results in reduced noise). The centerbody profile was designed to achieve lift from the forward section of the airfoil, with minimal loading on the aft section. This allows for a more efficient aircraft balance and reduced Mach numbers at the inlets to the engine, which enables more efficient boundary-layer ingestion [19]. The wing profile between the centerbody and outer wings was designed to minimize loading at the leading edge of the shoulder area of the planform, at which the outer wings meet the centerbody. The winglet profile is symmetric, and it was designed to minimize wave drag, as described in Sargeant [24].

C. Low-Speed Performance Analysis

The trimmed stall speed of the aircraft was estimated by combining a 2-D vortex lattice approach (AVL) and a viscous airfoil analysis (XFoil). In this approach, the aircraft angle of attack and elevator deflection for trim were iterated until the maximum airfoil sectional lift coefficient was reached. The design framework estimates stall and landing speed, landing-field length, and elevon deflection/thrust vectoring requirements for pitch trim during

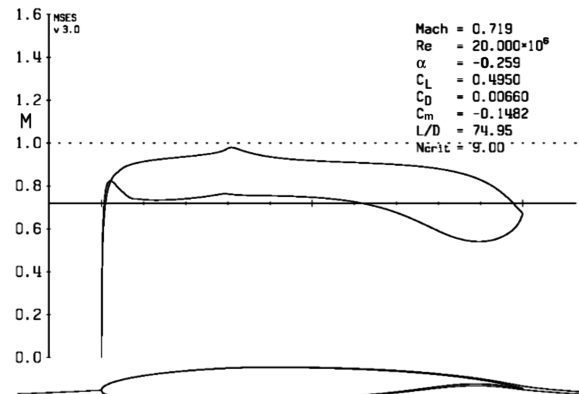


Fig. 7 Mach number distribution for the outer-wing section at cruise conditions for the SAX-40 aircraft design. Computed using MSES.

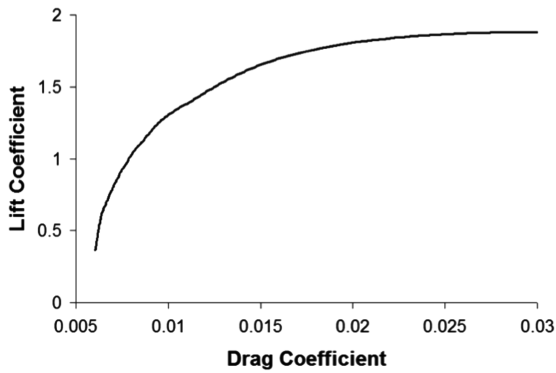


Fig. 8 Low-speed drag polar for the outer-wing section computed using XFOil. The use of a leading-edge droop increases $C_{L_{max}}$ to 2.2.

approach and landing. During takeoff, the elevon deflection/thrust vectoring requirements are assessed for rotation, and the aerodynamic performance is estimated during climbout. This analysis guided the propulsion-system design, as described in more detail in Crichton et al. [2,34], and it also provided an estimate for the airframe noise during takeoff and approach.

The aircraft dynamics during rotation, takeoff, and climbout were assessed using aerodynamic-performance parameters obtained from AVL and XFOil. In addition, the aircraft dynamic response to gusts and go-around maneuvers was analyzed. A detailed discussion and results can be found in companion papers [3,35].

D. Planform Optimization of Outer Wing

For the third generation of aircraft designs, constrained nonlinear optimization using sequential quadratic programming was carried out to optimize the outer-wing shape. The objective function was a linear combination of fuel efficiency and approach noise. As shown in Fig. 9, the variables defining the outer-wing shape included the leading-edge sweep, the wing chord at spanwise section five (spanwise location of 42.0 ft/12.8 m), the wing chord near the wing tip, and the outer-wing span. Constraints were placed on the maximum angle of attack at the beginning of cruise (less than 3 deg), the maximum leading-edge loading (ΔC_p less than 1.0), the minimum static margin at begin cruise (greater than 25 in.), the minimum distance between elevator and wing spar (greater than 0.3 ft/0.1 m), and the MTOW (less than 346,000 lb) to limit propulsion-system growth. The optimization routine used multiple wing shapes as initial condition. In addition, the weightings of fuel efficiency and approach airframe noise in the objective function were varied to yield a Pareto front of fuel efficiency versus approach airframe noise, for which the SAX-40 design was chosen. Specifically, the cost function was defined as

$$J = (1 - x) \cdot (100/\text{fuel efficiency}) + x \cdot (\text{noise}/57) \quad (10)$$

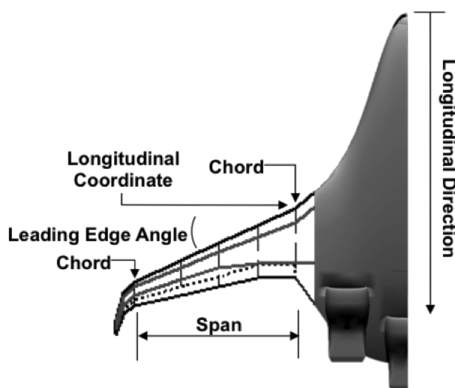


Fig. 9 Variables used in outer-wing shape optimization.

where

$$0 < x < 1$$

The Pareto front of designs that resulted from the optimization are presented in Sec. VI.A.

V. Design Methodology Validation

The validation of the design methodology consisted of a comparison between a 3-D Navier–Stokes solution and the results obtained from the quasi-3-D design methodology involving an Euler solution, a full panel solution, and a vortex lattice solution. The primary objective was to assess the fidelity of the design methodology in capturing the three-dimensionality of the viscous flow over the centerbody. A 3-D Navier–Stokes CFD analysis of the SAX-29 planform, using the CFL3DV6 code, was conducted at the Boeing Phantom Works. The assessment showed that the quasi-3-D design methodology is capable of capturing the major aerodynamic features, which demonstrates that the quasi-3-D design methodology is adequate for optimization purposes in which a rapid turnaround time is required. However, at the end of the optimization process, a fully viscous 3-D calculation should be created to evaluate the final design.

CFL3D [36] is a Navier–Stokes CFD code developed at NASA Langley Research Center for solving 2-D or 3-D flows on structured grids. The solution relied on the Spalart–Allmaras turbulence model and incorporated nearly 4 million grid cells. The analysis was conducted without winglets, and computations were conducted for flight Mach numbers ranging from 0.5 to 0.85 at angles of attack between 2.5 and 5.5 deg.

The aerodynamic loading characteristics of the SAX-29 airframe design are outlined in Fig. 10 for a cruise Mach number of 0.8. The loading contours from the 2-D vortex lattice code are qualitatively similar to the 3-D Navier–Stokes solution. Both solutions capture the centerbody loading due to the aerodynamic shaping of the leading edge region, the centerbody-wing junction loading, and the aft loading on the supercritical outer-wing sections. The solutions differ in the weak shock that forms on the outer wings. This is because the 2-D vortex lattice solution cannot capture shock waves, and compressibility effects are modeled with a Prandtl–Glauert correction. In the CFL3DV6 computation, the outer-wing shock is augmented by the presence of boundary layers that are not captured by the Euler or full-panel solutions. To capture the outer-wing shock in the quasi-3-D design methodology, 2-D viscous compressible airfoil calculations (MSES) are carried out on swept airfoil sections. An example is shown in subplot VI, in which the MSES solution is marked in gray. In the developed methodology, the outer-wing loading is estimated by the 2-D vortex lattice code and used to set the loading in the sectional viscous airfoil analysis (MSES). This approach breaks down for the highly 3-D flow near the centerbody (comparison not shown). Based on this assessment, inviscid 3-D full-panel solutions were generated for all subsequent designs to evaluate the aerodynamic loading.

The CFL3DV6 results for SAX-29 are shown in Fig. 11 and yield an ML/D of 16.7 at the begin-cruise lift coefficient of 0.197. The maximum ML/D of 17.3 occurs at a lift coefficient of 0.254. At the begin-cruise lift coefficient, the quasi-3-D design methodology overpredicts the CFL3DV6 estimate by 13%, which corresponds to a drag difference of 0.0011. The discrepancy is likely due to the methodology used to estimate the viscous drag on the centerbody, wherein the quasi-3-D design methodology relies on empirical drag estimates for bodies of revolution at a high Reynolds number, reported by Hoerner [29]. Furthermore, the CFL3DV6 calculations indicate that the SAX-29 airframe has the potential to achieve a maximum ML/D of 17.3 by operating at a higher-cruise Mach number of 0.83 (not shown in Fig. 11).

For the purposes of estimating the performance of the conceptual design, the developed quasi-3-D design methodology adequately captures the 3-D aerodynamic features and performance for optimization purposes. Based on the previous assessment, the

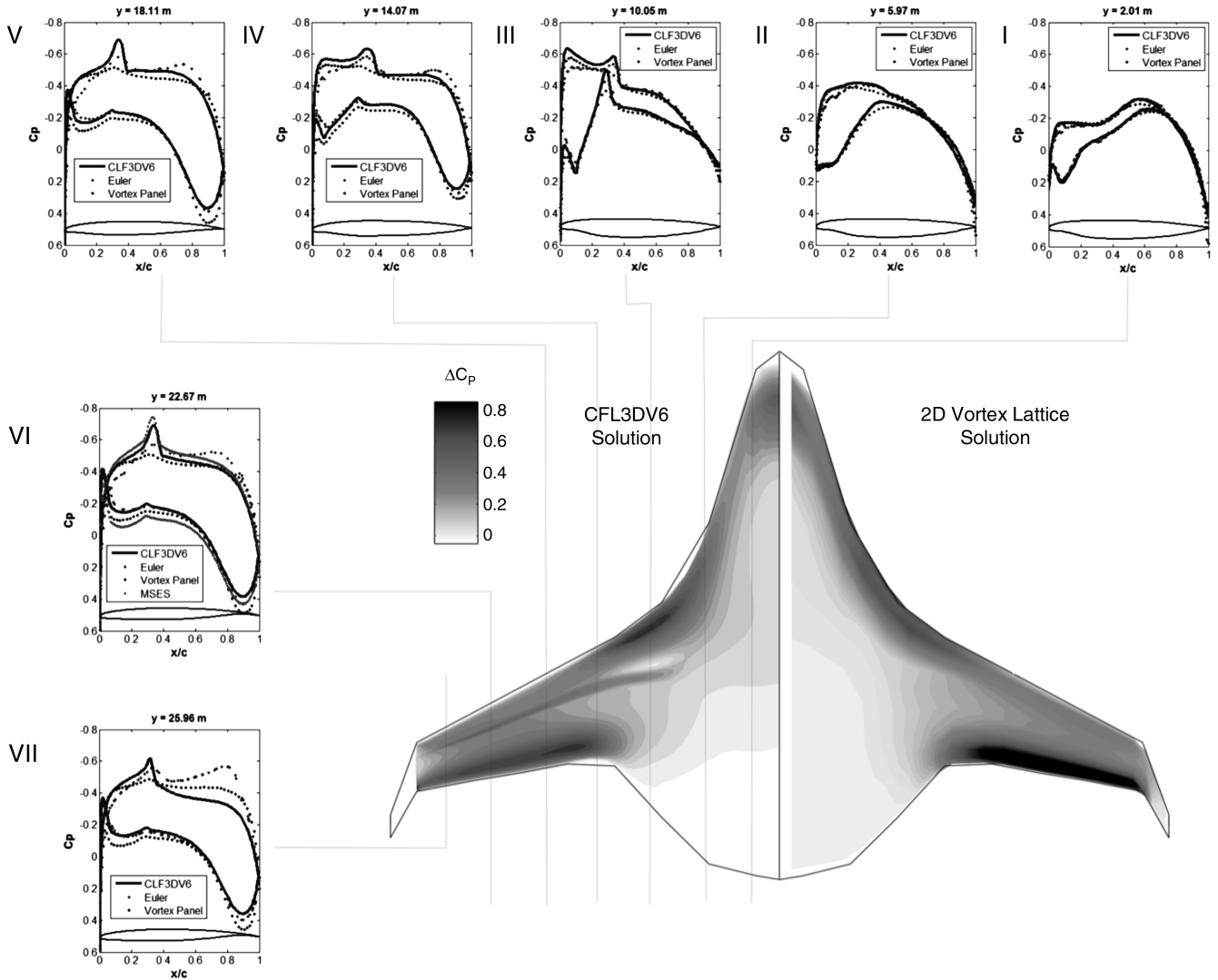


Fig. 10 3-D CFD validation of quasi-3-D design methodology: distribution and contours of pressure coefficient for SAX-29 airframe design (I–VII) at $M = 0.8$.

centerbody planform shape and airfoil profiles of the SAX-29 design were frozen in further design optimizations. Although mid- and outer-wing airfoil profiles could have been redesigned to eliminate the weak shock on the outer wing, and the 7% thickness of the outer wing may be insufficient for structural reasons, the profiles were deemed acceptable in the light of the relatively short project time frame.

VI. SAX-40 Aircraft Design

The SAX-40 conceptual aircraft design, shown in Fig. 1, was created based on the SAX-29 centerbody and airfoils, whereas the outer-wing planform and twist were optimized for low approach noise and high fuel efficiency at cruise. This section presents the aircraft design, with emphasis on the design strategies and their implications.

A. Noise–Fuel-Efficiency Design Space

The aircraft design space of noise and fuel efficiency, from which the SAX-40 design was selected, is shown in Fig. 12. This design space was created from the optimization of a large number of designs that spanned the full range of possible outer-wing planform shapes, as discussed in Sec. IV.D. The optimization cost function was chosen as a linear combination of approach noise and fuel efficiency, and the relative weightings were varied, such that each initial design was examined for five different cost functions, where x in Eq. (10) was varied from 0 to 1 in increments of 0.25.

Four designs are highlighted within the design space of Fig. 12, with select characteristics given in Table 1 to demonstrate the influence of the outer-wing properties on fuel efficiency and noise. Design A had minimum approach noise because its large wing area and shallow wing sweep allowed for reduced approach speeds (relative to the other designs). Design C, on the other hand, achieved better fuel efficiency at the expense of noise through increased wing sweep and decreased wing area. Design B achieved a compromise

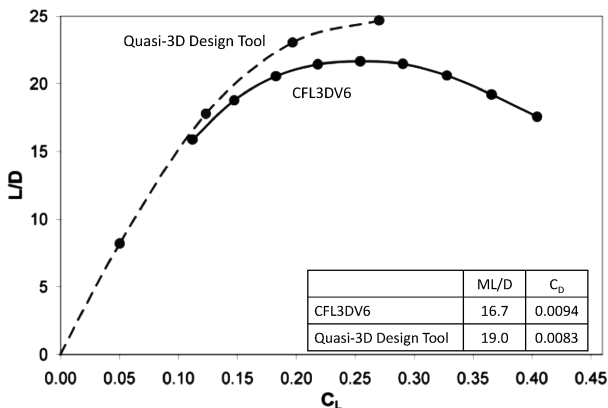


Fig. 11 Comparison of SAX-29 performance estimates at $M = 0.8$: quasi-3-D design methodology and CFL3DV6 calculation.

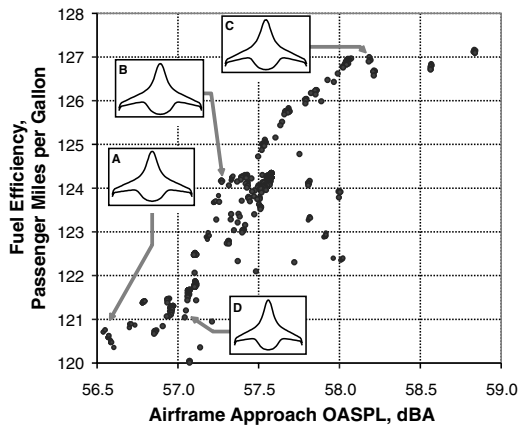


Fig. 12 Fuel efficiency and noise design space from which the SAX-40 design was chosen (OASPL denotes overall sound pressure level).

between these designs, and it was selected as the SAX-40 design. Design D was highlighted, because it meets the wingspan requirements for an International Civil Aviation Organization (ICAO) class E airport [Federal Aviation Administration (FAA) group V] [37]. The other designs have wingspans exceeding 65.0 m (213.3 ft), thus limiting their operation to ICAO class F airports (FAA group VI), which allow aircraft with wingspans up to 80.0 m (262.5 ft). The penalty for the reduced wingspan of Design D is a 2% decrease in fuel efficiency.

B. Aerodynamic Performance

The geometry and performance of the SAX-40 are given in Tables 2–4. Using the quasi-3-D design methodology, the ML/D is calculated to be 20.1 at the beginning of cruise. Because of time constraints, a fully viscous 3-D CFD analysis of the SAX-40 could not be conducted. If the ML/D is overpredicted by 13%, as discussed previously for the SAX-29, the ML/D at beginning cruise would reduce to 17.5. In comparison, an ML/D of 18 is reported for the BWB design by Liebeck [4], of 15.5 for the Boeing 777 [38], and of 13.4 for the BWB by Qin et al. [39].

As illustrated by the planform comparison in Fig. 3, the optimizer redistributed the wing area by removing chord from the mid-wing region at a spanwise location of about 40 ft (12.2 m) and by increasing the overall wing span. This led to a 6% increase in ML/D between the SAX-29 and the SAX-40.

C. Weight and Balance

The aircraft weight buildup, presented in Table 5, includes a design payload for 215 pax at 240 lb per pax (108.8 kg/pax), 20 lb per pax heavier than mandated by FAA Advisory Circular 120-27E [40]. If the passengers were each allocated 220 lb (99.8 kg), then the aircraft could carry 236 pax, or 215 pax with 4300 lb (1950 kg) of revenue cargo.

One of the challenges inherent in scaling the SAX and other all-lifting body airframe designs to shorter range or smaller payload is the high empty-weight fraction, OEW over MTOW. In the Breguet range equation the empty weight fraction, along with ML/D and specific fuel consumption, determines the aircraft fuel efficiency. The SAX-40 weight fraction of 0.62 is higher in comparison with conventional aircraft configurations. For example, the Boeing 767-300 introduced in 1982, an aircraft with a similar mission to the SAX-40, has a weight fraction of 0.52 [38].

D. Internal Layout

The internal configuration of the aircraft design is presented from three views in Fig. 13. The interior of the SAX-40 cabin was not designed in detail, but the outer cabin shape was used as a constraint in the planform and airfoil design optimization. More specifically, as shown in Fig. 14, the outer skin was required to enclose the passenger

cabin, the cargo bay, and the spar box. The original cabin dimensions were set by WingMOD, which then grew as the planform area increased by incorporating the aerodynamic shaping of the centerbody leading edge. The SAX-40 cabin has 2570 ft² (239 m²) of floor area. With 215 pax, the cabin passenger density is 0.9 pax/m². In comparison, the Boeing 767-300 and 767-400 have passenger densities of 1.4 pax/m² in a dual-class configuration [41]. The SAX-40 cabin could carry 335 pax at this density. The cabin was defined as a box with a height of 6.6 ft (2.0 m), but as shown in the side view of Fig. 13, there is much space between the cabin top and aircraft skin, such that the cabin height could be increased up to 9.7 ft (3.0 m).

The SAX-40 cargo bay was set at 39.4 × 16.4 × 4.6 ft, which yields a volume of 2970 ft³ (12.0 × 5.0 × 1.4 m and 84.1 m³). The fuel tank capacity of 12,000 gal (80,000 lb/36,000 kg) is provided via two inner-wing tanks close to the aircraft center of gravity. Fuel pumping is not necessary to maintain static stability. The planform has considerable empty space in the wings that can potentially be used to carry additional fuel for increased range. However, this additional fuel would lead to a larger thrust requirement on takeoff, which in turn would increase noise. The faired dual-four-wheel main-gear bogeys are stowed behind the cargo bay, whereas the simple dual-wheel nose gear retracts forward into the fuselage. The embedded propulsion system is shown to scale in the figures, and the engine-fan faces are marked to indicate the inlet duct length.

E. Pitch Trim and Static Stability

The outer-wing profile configuration and loading distribution obtained from the 2-D vortex lattice solution for approach and cruise conditions are shown in Fig. 15. For reference, the centerbody profile is shown to scale, and the dot indicates the aircraft center of gravity. The supercritical airfoils on the outer wing are twisted 3.5 deg outwash, such that at the beginning of cruise, the outer-wing loading is concentrated aft of the aircraft center of gravity. This loading is naturally balanced by the lift generated in the forward region of the centerbody. As fuel is burned from the beginning to the end of cruise, the thrust angle is increased for pitch trim. A maximum-thrust vectoring angle of 10.5 deg is reached at the end of cruise. Thrust vectoring is preferred over deflecting elevators in order to keep the cabin angle below 3 deg. **Elevator deflections for pitch trim unload the outer wings, such that the aircraft angle of attack has to increase to maintain steady flight. However, thrust vectoring would incur a weight penalty and adds complexity to the design.

At begin cruise, a positive 5.9% static margin is estimated using the 2-D vortex lattice solution. This corresponds to a distance between the center of gravity and the center of pressure of 31 in., which exceeds the expected 25 in. travel of the passenger and cargo center of gravity. As fuel is burned during cruise, the center of gravity moves forward, and the static margin increases to 9.5% (equivalent to 50 in.). In comparison, the BWB reported in Liebeck [4] has a positive static margin of 5% while trimmed at cruise.

The SAX-40 suction and pressure-surface C_p distributions from the full-panel solution at cruise conditions show similar trends to those of Fig. 15. The loading due to the aerodynamic shaping of the centerbody leading edge is evident in the increased pressure coefficient in the forward region. The centerbody airfoil design has minimal aft camber in order to avoid an untrimmable nose-down moment. This also results in an enhanced external precompression of the flow upstream of the engine inlets, mitigating the aerodynamic challenge of integrating the propulsion system into the airframe. A detailed discussion of the engine integration and inlet design can be found in Plas et al. [6].

F. Low-Speed Capability

The change in planform depicted in Fig. 3 resulted in a decrease in stall speed from 118 kt (63.8 m/s) for the SAX-12 to 96.0 kt (49.4 m/s) for the SAX-40. The stall speeds were estimated at the

**S. Wakayama, Boeing Phantom Works, Dec. 2006, Personal Communication.

Table 1 Characteristics of the four aircraft designs highlighted in Fig. 12

	Midchord sweep, deg	Span, m/ft	Span (with winglets), m/ft	Area, m ² /ft ²	Fuel efficiency, pax · mile/gal	Airframe approach OASPL, dBA
A	16.9	62.0/203	66.2/217	850.4/9154	120.7	56.5
B	19.3	63.2/207	67.5/221	836.0/8998	124.2	57.3
C	20.0	63.9/210	68.3/224	829.9/8933	127.0	58.2
D	16.8	60.8/199	65.0/213	840.4/9046	121.0	57.0

Table 2 SAX-40 geometric parameters

Parameter	Value
Wing area, m ² /ft ²	836.0/8998
Wing span, m/ft	63.22/207.4
Cruise Mach	0.8
Outer-wing twist, deg	-3.25
Stall speed, m/s/kt	49.4/96.0

Table 3 SAX-40 aerodynamic performance parameters

Parameter	Begin cruise	End cruise
Cruise altitude, ft	40,000	45,000
Lift coefficient	0.2064	0.2091
Angle of attack, deg	2.7	2.7
C.g., % centerbody chord	58.3	57.1
Static margin, %/in.	5.9/31	9.5/50
Elevator deflection, deg	0	0
Thrust vector angle, deg	0	10.5 up
ML/D	20.1	18.8

Table 4 SAX-40 lift, moment, and drag coefficients at beginning of cruise

Coefficient	Value
C_L	0.2064
C_D	0.0082
C_{Di}	0.0024
C_{Dp}	0.0009
C_{Dp} centerbody	0.0004
C_{Dp} wing	0.0005
C_{Df}	0.0045
C_{Df} centerbody	0.0027
C_{Df} wing	0.0018
C_D wave	0.0001
C_D , engine nacelles	0.0004

Table 5 SAX-40 aircraft weight buildup

Component	Mass, kg/lb
MTOW	150,850/332,560
OEW	94,190/207,660
Design payload	23,400/51,600
Fuel with reserves	33,250/73,310
Structure	47,570/104,870
Fixed equipment	23,230/51,220
Landing gear	6700/14,760
Propulsion	16,700/36,810

nominal landing weight, which included the design payload and the reserve fuel. For comparison, aircraft of similar weight to the SAX-40 have typical stall speeds of 114 to 130 kt, which correspond to approach speeds of 140 to 160 kt (72 to 82 m/s) [3]. According to FAR 25.125 [42], the approach speed must exceed 1.23 times the stall speed. The stall speed can be reduced by decreasing the sweep angle Λ , but this also incurs a cruise wave drag penalty. The tradeoffs can

be considered in terms of the infinite swept wing theory, in which the flow in the airfoil plane normal to the spanwise axis sees a reduced Mach number M and a reduced dynamic pressure q :

$$M_{\perp} = M \cos(\Lambda) \tag{11}$$

$$q_{\perp} = q \cos^2(\Lambda) \tag{12}$$

The resulting perpendicular 2-D airfoil coefficients, $c_{l,max}$ and $c_{d,pressure}$, then give the 3-D aircraft coefficients as follows:

$$C_{L,max} = c_{l,max} \cos^2(\Lambda) \tag{13}$$

$$C_{D,pressure} = c_{d,pressure} \cos^3(\Lambda) \tag{14}$$

These quantify the effect of the sweep angle Λ on $C_{L,max}$ (hence the stall speed) and on the wave drag, which is a part of $C_{D,pressure}$. The

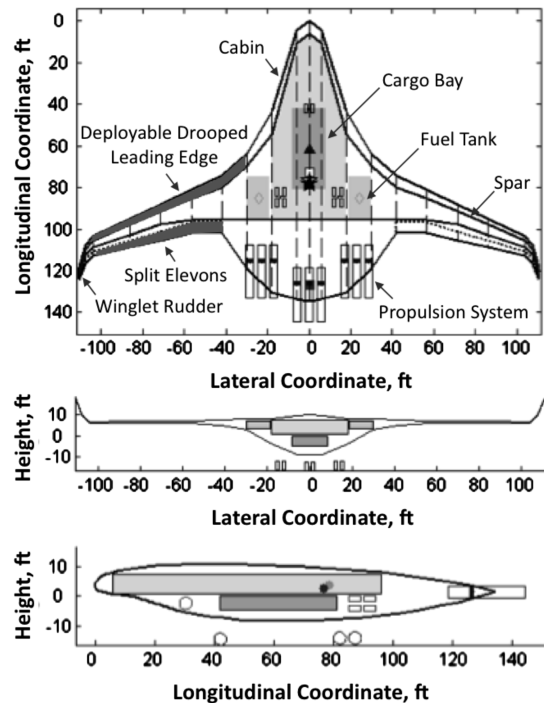


Fig. 13 Internal layout illustrating cabin, cargo, fuel tanks, spars, propulsion system, and undercarriage.

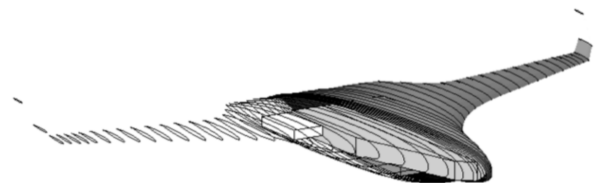


Fig. 14 Internal layout illustrating cabin, cargo, and fuel tanks; all are given relative to the aircraft outer skin, which is shown via the spatial distribution of airfoil profiles.

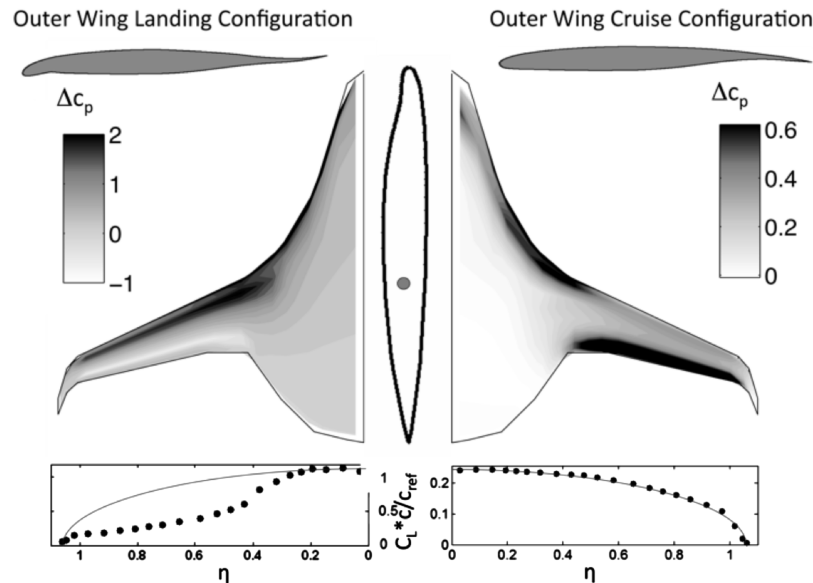


Fig. 15 2-D vortex lattice estimate of airframe loading distribution during cruise and approach/landing.

optimization reached a compromise between cruise performance and stall speed at a midchord sweep of 19 deg.

During approach and in low-speed flight, the SAX-40 aircraft is trimmed by combining thrust vectoring and elevon deflections. Downward-vectoring idle thrust at 30 deg and simultaneously upward-deflected elevons at 18.5 deg unload the outer-wing trailing-edge region and require a large angle of attack to generate the necessary lift. A drooped leading edge is implemented to achieve an angle of attack of 15.6 deg. A detailed assessment of the high-lift system can be found in Andreou et al. [43,44]. The experimental study demonstrates that the noise radiated from drooped leading edges is comparable with the levels of airfoil self-noise. The consequence of the high-angle-of-attack configuration is a nonelliptic lift distribution generating sufficient induced drag to trim the aircraft on a 3.9 deg flight-path angle. The SAX-40 aircraft could also fly a 3 deg flight-path angle on approach, with a noise level of 63 dBA at the airport perimeter. To demonstrate glide-slope capture at a 6 deg flight-path angle (necessary for certification), split elevons act as drag rudders in nonsilent operation. A potential additional benefit of unloading the aft outer wings could be reduced power requirements for elevon operation.

The SAX-40 airframe was designed for low stall speed to reduce the airframe noise on approach. This inherently leads to enhanced low-speed performance during takeoff. At takeoff, thrust vectoring is used for pitch trim, because elevon deflections decrease the aircraft L/D and deteriorate the climbout performance. To rotate the aircraft at takeoff, the elevons are deflected in combination with vectored thrust [2].

G. Fuel Efficiency

The SAX-40 aircraft design has the potential for large reductions in fuel efficiency. A fuel efficiency of 124 pax miles per gallon (0.65 MJ per available seat kilometer) was calculated and compared with aircraft fuel-efficiency data from Lee et al. [38] and Peeters et al. [45] in Fig. 16. The estimated SAX-40 fuel efficiency is 28% better than a Boeing 777 with a cabin configuration that delivers maximum passenger miles per gallon. For further comparison, a Toyota Prius hybrid automobile with two occupants would achieve 120 pax miles per gallon [46].

When the productivity being delivered by the movement of cargo is taken into account, the SAX-40 aircraft has comparable efficiency to a Boeing 777. The SAX-40 payload fuel energy intensity and fuel energy consumed per payload (mass · range) was estimated as 5.9 kJ/kg · km, slightly worse than a Boeing 777-200, which has a payload fuel energy intensity of 5.7 kJ/kg · km (both were estimated at the maximum range with maximum structural payload). This result

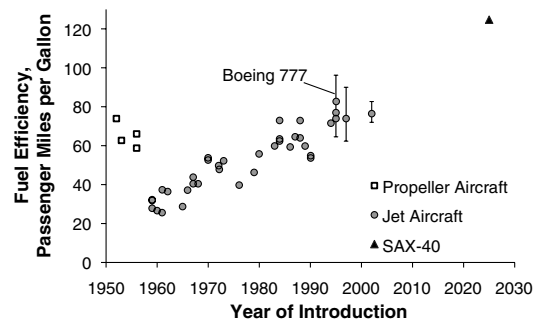


Fig. 16 Fuel efficiency of SAX-40 in relation to current and past commercial passenger aircraft. Existing and past aircraft fuel efficiencies based on energy use estimates (energy per available seat kilometer) with an assumed fuel energy content of 34.6 MJ/L [47]. The uncertainty bands represent variation in passenger configuration [38,45].

points to the efficiency of modern long-range aircraft in moving passengers and cargo, a fact that is not captured in the comparison shown in Fig. 16. However, the cargo space on most modern passenger operations is not being fully used, as the cargo load factor of passenger operations was only 16% in 2007 [47]. For comparison, the cargo capacity of the SAX-40 aircraft with 215 pax, 4300 lb, is roughly a tenth of that of a Boeing 777-200. To ensure consistency, the cargo capacity of the Boeing 777-200 was assumed to be the maximum structural payload weight minus 400 pax at 220 lb apiece. All of the Boeing 777-200 data were derived from The Boeing Company's airline planning guides. Because roughly one-eighth of the payload mass carried by aviation is revenue cargo, either in the belly of passenger aircraft or in dedicated freighter aircraft, additional analysis is required to determine whether or not reduced-cargo-capacity passenger aircraft would improve fleetwide fuel efficiency, as measured on a payload mass · range basis [47].

The SAX-40 fuel-efficiency estimates are based on a specific fuel consumption of 0.49 lb/lb · h, which includes the effect of boundary-layer ingestion. A detailed discussion of propulsion-system performance for this highly integrated configuration can be found in de la Rosa Blanco et al. [9] and Plas et al. [6].

H. Aircraft Noise

The aircraft approach velocity for SAX-40 is calculated to be 28% lower than the typical approach velocity for similar-sized aircraft. This improvement in low-speed flight capability contributes

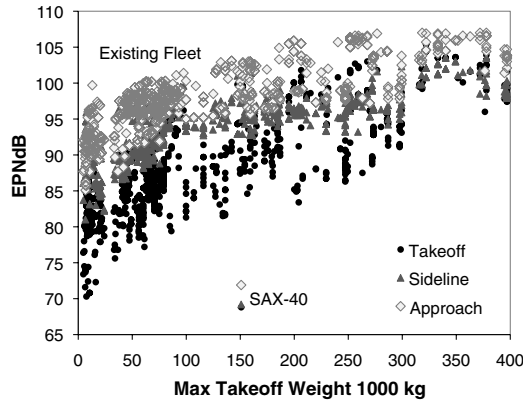


Fig. 17 Estimated EPNL for the SAX-40 aircraft with the Granta-3401 propulsion system in comparison to U.S.-certified jet-powered airplanes [48,49].

significantly to the overall reduction in noise: the calculated noise level at the airport perimeter of 62 dBA is near the background noise of a well-populated area. As shown in Fig. 17, and discussed at length in two companion papers focused on the assessment of takeoff noise [2] and approach noise [3], a reduction in cumulative noise (sideline, takeoff, and approach) of 75 EPNdB in the cumulative effective perceived noise level (EPNL) is estimated relative to the ICAO chapter 4 requirement of 284.5 cumulative EPNdB. The EPNL value was computed according to the FAA procedures documented in part 36 [48,49]. Tone corrections were neglected, because tonal noise could not be computed for the airframe noise sources.

Two sources of uncertainty, structural weight and aerodynamic performance, were examined using the design methodology to determine their influence on the fuel efficiency and noise emission of the final aircraft design. Table 6 shows the impact of uncertainty in the aerodynamic performance of the design methodology used to estimate the SAX-40 fuel efficiency. The MTOW was kept constant for this analysis, and the design range was decreased. Adding five counts of drag has similar impact to adding 10,000 lb (4500 kg) of weight, whereas adding 10 counts of drag could reduce the fuel efficiency by 12% and the range by 13%. Under this scenario, the performance of the aircraft would be degraded, but it would still achieve silence at the airport perimeter with fuel efficiency that is 10% better than current designs.

The noise–fuel–efficiency design space of Fig. 12 has been expanded in Fig. 18 to include aircraft designs that were created with a 10% increase in the structure weight. To maintain a constant MTOW and avoid an engine redesign, the design range of the increased-weight aircraft was set at 4500 nm. Thus, a 10% increase in structural weight could result in a 10% reduction in range and a 5% reduction in fuel efficiency. However, the noise level of the SAX-40 would still be achieved as the approach airframe noise is unchanged, as are the engine design and MTOW.

I. Sensitivity Studies

Two sources of uncertainty, structural weight and aerodynamic performance, were examined using the design methodology to determine their influence on the fuel efficiency and noise emission of the final aircraft design. Table 6 shows the impact of uncertainty in the aerodynamic performance of the design methodology used to estimate the SAX-40 fuel efficiency. The MTOW was kept constant

Table 6 Influence of increased drag on the performance estimates of the SAX-40 design

C_D	ML/D	Range, nm	Fuel efficiency, pax · nm/gal
+0.0000	20.1	5,000	124
+0.0005	18.9	4,650	116
+0.0010	17.9	4,350	109
+0.0015	16.9	4,100	103

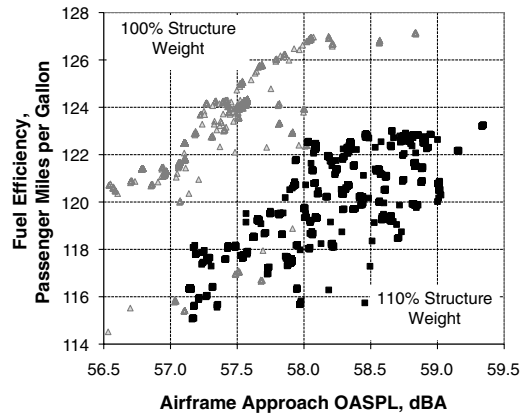


Fig. 18 Influence of increased structural weight on the SAX-40 fuel efficiency and noise design space.

for this analysis, and the design range was decreased. Adding five counts of drag has similar impact to adding 10,000 lb (4500 kg) of weight, whereas adding 10 counts of drag could reduce the fuel efficiency by 12% and the range by 13%. Under this scenario, the performance of the aircraft would be degraded, but it would still achieve silence at the airport perimeter with fuel efficiency that is 10% better than current designs.

The noise–fuel–efficiency design space of Fig. 12 has been expanded in Fig. 18 to include aircraft designs that were created with a 10% increase in the structure weight. To maintain a constant MTOW and avoid an engine redesign, the design range of the increased-weight aircraft was set at 4500 nm. Thus, a 10% increase in structural weight could result in a 10% reduction in range and a 5% reduction in fuel efficiency. However, the noise level of the SAX-40 would still be achieved as the approach airframe noise is unchanged, as are the engine design and MTOW.

VII. Conclusions

A quasi-3-D design methodology was developed for the conceptual design of an aircraft with step changes in noise reduction and fuel efficiency. The design methodology was validated using a fully viscous 3-D CFD calculation and was subsequently used in an aircraft-design-optimization framework. The key feature of the resulting aircraft design, the SAX-40, is the aerodynamically shaped leading edge of the airframe centerbody. The all-lifting airframe is optimized to generate a lift distribution that balances aerodynamic moments for pitch trim and static stability, achieves an elliptical span load on cruise, and increases the induced drag on approach, reducing the stall speed.

The conceptual aircraft design yields a cruise ML/D of 20.1 and a potential fuel efficiency of 124 pax miles per gallon. The trimmed approach speed is calculated to be 28% lower than existing commercial aircraft, enabling a step change in airframe noise reduction. The estimated maximum noise level at the airport perimeter is 62 dBA, which corresponds to a computed 75 cumulative EPNdB reduction, relative to the ICAO chapter 4 requirements. The economic analysis of a silent aircraft is presented in companion works [50,51].

Some of the technologies introduced yield a number of technical challenges and are of considerable risk. These must be overcome before this design concept can become a reality. For example, the pressure vessel and structural integrity of the unconventional all-lifting body pose challenges in fabrication and manufacturing. The low-speed aerodynamics of the airframe need to be assessed using 3-D viscous flow computations, and the stowage and implementation of a faired undercarriage need to be further analyzed. A major challenge is the integration of the distributed propulsion system in the airframe. Inlet distortion noise and forced vibration issues due to nonuniform inlet flow must be resolved, and the mechanical challenges of the geared fan transmission system and the variable area thrust vectoring exhaust nozzles must be overcome.

In summary, the SAX-40 conceptual aircraft design meets the objectives of a silent and fuel-efficient aircraft, although there is considerable risk embedded in the choice of technologies used in the design.

Acknowledgments

This research was funded by the Cambridge–MIT Institute, which is gratefully acknowledged. The authors thank The Boeing Company group in Seattle for fruitful discussions on center-of-gravity travel. Without the experience and encouragement of Bob Liebeck, Dino Roman, and Sean Wakayama at the Boeing Phantom Works, the aircraft design presented in this paper could not have been achieved. Their continuous support and the CFL3DV6 analysis conducted by Dino Roman are gratefully acknowledged. The authors are also indebted to many members of the Silent Aircraft Initiative who have been instrumental in the completion of this work. Special thanks go to Dan Crichton for conducting the takeoff effective perceived noise level calculations, Steven Thomas for providing the renderings of the aircraft designs, and Karen Willcox for her assistance in the area of BWB-type design and optimization. Matthew Sargeant is grateful to the Cambridge Australia Trust for his doctoral fellowship.

References

- [1] Manneville, A., Pilczner, D., and Spakovszky, Z., "Preliminary Evaluation of Noise Reduction Approaches for a Functionally Silent Aircraft," *Journal of Aircraft*, Vol. 43, No. 3, 2006, pp. 836–840. doi:10.2514/1.16424
- [2] Crichton, D., de la Rosa Blanco, E., Law, T., and Hileman, J., "Design and Operation for Ultra Low Noise Take-Off," AIAA Paper 2007-0456, 2007.
- [3] Hileman, J. I., Reynolds, T. R., de la Rosa Blanco, E., and Law, T., "Development of Approach Procedures for Silent Aircraft," AIAA Paper 2007-0451, 2007.
- [4] Liebeck, R. L., "Design of the Blended-Wing-Body Subsonic Transport," *Journal of Aircraft*, Vol. 41, No. 1, 2004, pp. 10–25. doi:10.2514/1.9084
- [5] Diedrich, A., Hileman, J., Tan, D., Willcox, K., and Spakovszky, Z., "Multidisciplinary Design and Optimization of the Silent Aircraft," AIAA Paper 2006-1323, 2006.
- [6] Plas, A. P., Madani, V., Sargeant, M. A., Greitzer, E. M., Hall, C. A., and Hynes, T. P., "Performance of a Boundary Layer Ingesting Propulsion System," AIAA Paper 2007-0450, 2007.
- [7] Hall, C. A., and Crichton, D., "Engine and Installation Configurations for a Silent Aircraft," AIAA Paper 2005-1164, 2005.
- [8] Hall, C. A., and Crichton, D., "Engine Design Studies for a Silent Aircraft," *ASME Turbo Expo*, American Society of Mechanical Engineers Paper GT2006-90559, New York, May 2006.
- [9] de la Rosa Blanco, E., Hall, C., and Crichton, D., "Challenges in the Silent Aircraft Engine Design," AIAA Paper 2007-0454, 2007.
- [10] Agarwal, A., and Dowling, A., "A Ray Tracing Approach to Calculate Acoustic Shielding by the Silent Aircraft Airframe," AIAA Paper 2006-2618, 2006.
- [11] Law, T., and Dowling, A., "Optimization of Traditional and Blown Liners for a Silent Aircraft" AIAA Paper 2006-2525, 2006.
- [12] Quayle, A., Dowling, A., Babinsky, H., Graham, W., and Sijtsma, P., "Landing Gear for a Silent Aircraft," AIAA Paper 2007-0231, 2007.
- [13] Quayle, A. R., "Landing Gear for a Silent Aircraft," Ph.D. Dissertation, Engineering Department, Univ. of Cambridge, Cambridge, England, U.K., 2008.
- [14] Sakaliyski, K. D., Hileman, J. I., and Spakovszky, Z. S., "Aeroacoustics of Perforated Drag Plates for Quiet Transport Aircraft," AIAA Paper 2007-1032, 2007.
- [15] Shah, P., Mobed, D., and Spakovszky, Z. S., "Engine Air-Brakes for Quiet Transport Aircraft," AIAA Paper 2007-1033, 2007.
- [16] Lilley, G. M., "The Prediction of Airframe Noise and Comparison with Experiment," *Journal of Sound and Vibration*, Vol. 239, No. 4, 2001, pp. 849–859. doi:10.1006/jsvi.2000.3219
- [17] Herr, M., and Dobrzyński, W., "Experimental Investigations in Low-Noise Trailing-Edge Design," *AIAA Journal*, Vol. 43, No. 6, 2005, pp. 1167–1175. doi:10.2514/1.11101
- [18] Lockard, D. P., and Lilley, G. M., "The Airframe Noise Reduction Challenge," NASA TM-2004-213013, 2004.
- [19] Sargeant, M. A., Hynes, T. P., Graham, W. R., Hileman, J. I., Drela, M., and Spakovszky, Z. S., "Stability in Blended Wing Body Type Aircraft with Centerbody Leading Edge Carving," *Journal of Aircraft*, Vol. 47, No. 3, 2010, pp. 970–974. doi:10.2514/1.46544
- [20] Wakayama, S., "Blended-Wing-Body Optimization Problem Setup," AIAA Paper 2000-4740, 2000.
- [21] Hileman, J. I., Spakovszky, Z. S., Drela, M., and Sargeant, M., "Aerodynamic and Aeroacoustic Three-Dimensional Design for a 'Silent' Aircraft," AIAA Paper 2006-0241, 2006.
- [22] "Newpan Overview," Flow Solutions, South Gloucestershire, England, U.K., 2006. <http://www.flowsol.co.uk/products/newpan/> [retrieved Dec. 2006].
- [23] Jones, A., "Multidisciplinary Optimization of Aircraft Design and Takeoff Operations for Low Noise," S.M. Thesis, Department of Aeronautics and Astronautics, Massachusetts Inst. of Technology, Cambridge, MA, 2006.
- [24] Sargeant, M. A., "Boundary Layer Ingestion for Advanced Airframes," Ph.D. Dissertation, Department of Engineering, Univ. of Cambridge, 2007.
- [25] Drela, M., and Youngren, H., "AVL Overview" [online product brochure], <http://web.mit.edu/drela/Public/web/avl/> [retrieved Oct. 2004].
- [26] Drela, M., and Giles, M. B., "Viscous-Inviscid Analysis of Transonic and Low Reynolds Number Airfoils," *AIAA Journal*, Vol. 25, No. 10, 1987, pp. 1347–1355. doi:10.2514/3.9789
- [27] Drela, M., "Design and Optimization Method for Multielement Airfoils," AIAA Paper 93-0960, 1993.
- [28] Drela, M., "MSES Multi-Element Airfoil Design/Analysis Software: Summary" [online product brochure], 16 May 2004, <http://raphael.mit.edu/drela/msessum.ps> [retrieved 12 Nov. 2005].
- [29] Hoerner, S. F., *Fluid Dynamic Drag*, Hoerner Fluid Dynamics, Bakersfield, CA, 1965.
- [30] Raymer, D. P., *Aircraft Design: A Conceptual Approach*, 3rd ed., AIAA Education Series, AIAA, Reston VA, 1999.
- [31] Wakayama, S., and Kroo, I., "Subsonic Wing Planform Design Using Multidisciplinary Optimization," *Journal of Aircraft*, Vol. 32, No. 4, 1995, pp. 746–753. doi:10.2514/3.46786
- [32] Diedrich, A., "The Multidisciplinary Design and Optimization of an Unconventional, Extremely Quiet Aircraft," S.M. Thesis, Department of Aeronautics and Astronautics, Massachusetts Inst. of Technology, Cambridge, MA, 2005.
- [33] Roskam, J., *Airplane Design, Part 5: Component Weight Estimation*, 2nd ed., Roskam Aviation and Engineering Corp., Ottawa, KS, 1989, pp. 97–112.
- [34] Crichton, D., "Fan Design and Operation for Ultra Low Noise," Ph.D. Dissertation, Department of Engineering, Univ. of Cambridge, 2007.
- [35] Thomas, S., and Dowling, A., "A Dynamical Model and Controller for the Silent Aircraft," AIAA Paper 2007-0866, 2007.
- [36] Rumsey, C. L., "CFL3D Version 6 Home Page," NASA, 31 Aug. 2006, <http://cfl3d.larc.nasa.gov/Cfl3dv6/cfl3dv6.html> [retrieved Dec. 2006].
- [37] "Airport Design," Federal Aviation Administration Advisory Circular 150/5300-13, Chap. 1, Sec. 2, Oct. 2002.
- [38] Lee, J. J., Lukachko, S. P., Waitz, I. A., and Schafer, A., "Historical and Future Trends in Aircraft Performance, Cost and Emissions," *Annual Review of Energy and the Environment/AR*, Vol. 26, No. 1, 2001, pp. 167–200. doi:10.1146/annurev.energy.26.1.167
- [39] Qin, N., Vavalle, A., Le Moigne, A., Laban, M., Hackett, K., and Weinerfelt, P., "Aerodynamic Considerations of Blended-Wing-Body Aircraft," *Progress in Aerospace Sciences*, Vol. 40, No. 6, 2004, pp. 321–343. doi:10.1016/j.paerosci.2004.08.001
- [40] "Aircraft Weight and Balance Control," Federal Aviation Administration, Advisory Circular 120-27E, Chap. 2, Sec. 2, June 2005.
- [41] "767-400ER Airplane Characteristics for Airport Planning," The Boeing Co., Commercial Airplanes Group Rept. D6-58238-1, Chicago, Nov. 2000.
- [42] "Part 25 Airworthiness Standards: Transport Category Airplanes, Landing," Federal Aviation Administration Regulation Sec. 25.125, 2002.
- [43] Andreou, C., Graham, W., and Shin, H.-C., "Aeroacoustic Study of Airfoil Leading Edge High-Lift Devices," AIAA Paper 2006-2515, 2006.
- [44] Andreou, C., "Acoustic and Aerodynamic Properties of Aerofoil Leading-Edge High-Lift Geometries," Ph.D. Dissertation, Department of Engineering, Univ. of Cambridge, Cambridge, England, U.K., 2008.

- [45] Peeters, P. M., Middel, J., and Hoolhorst, A., "Fuel Efficiency of Commercial Aircraft: An Overview of Historical and Future Trends," National Aerospace Laboratory, NRL-CR-2005-669, The Netherlands, 2005.
- [46] "Toyota Prius Specifications," Toyota Motor Sales, U.S.A., Torrance, CA, 2005, <http://www.toyota.com/prius/specs.html> [retrieved Dec. 2006].
- [47] Hileman, J. I., Katz, J. B., Mantilla, J. G., and Fleming, G., "Payload Fuel Energy Efficiency as a Metric for Aviation Environmental Performance," *Proceedings of the 26th International Congress of the Aeronautical Sciences*, Anchorage, AK, Sept. 2008, pp. 1-11.
- [48] "Part 36, Noise Standards: Aircraft Type and Airworthiness Certification," Federal Aviation Administration, Electronic Code of Federal Regulations (e-CFR) Title 14, Chap. 1, Subchap. C, Part 36, Nov. 2006.
- [49] "Noise Levels for U. S. Certificated and Foreign Aircraft. Appendix 1: U.S. Certificated Turbojet Powered Airplanes," Federal Aviation Administration AC36-1H, Nov. 2001 http://www.faa.gov/about/office_org/headquarters_offices/aep/noise_levels/ [retrieved Dec. 2006].
- [50] Tam, R., Belobaba, P., Polenske, K. R., and Waitz, I., "Assessment of Silent Aircraft-Enabled Regional Development and Airline Economics in the U.K.," AIAA Paper 2007-455, 2007.
- [51] Tam, R., "Regional Catalytic Economic Impacts and Noise-Damage Costs of Aviation Growth," Ph.D. Dissertation, Department of Urban Studies and Planning, Massachusetts Inst. of Technology, Cambridge, MA, 2008.